



CENTRIFUGE MODEL TESTS FOR A SUBMARINE SLOPE DURING AN EARTHQUAKE AND ITS SLOPE STABILITY ANALYSIS

K. Saito⁽¹⁾, N. Sento⁽²⁾, S. Nakamura⁽³⁾

(1) Master student, Department of Civil Engineering, Graduate School Engineering, Nihon University, ceka18003@g.nihon-u.ac.jp

(2) Professor, Department of Civil Engineering, College of Engineering, Nihon University, sentou.noriaki@nihon-u.ac.jp

(3) Professor, Department of Civil Engineering, College of Engineering, Nihon University, s-nak@civil.ce.nihon-u.ac.jp

Abstract

Submarine landslides triggered by earthquakes cause tsunamis. The largest contributors to the height of a tsunami are the volume and velocity of the sliding mass. Therefore, to enable accurate predictions of tsunami elevation, it is important to elucidate the failure behavior of submarine slopes during earthquakes. This study evaluated the collapse behavior of a submarine slope during an earthquake by performing a series of centrifugal model tests. Additionally, the validation of applying the modified Fellenius method to submarine slopes was investigated. The slopes were composed of kaolinite clay, with slope angles of 15°, 30°, and 35°. A series of tests were conducted at a centrifugal acceleration of 30 G with water depths of 15 and 23 m. Sinusoidal waves of 10 cycles each were applied, with amplitudes increasing from 0.5 to 3.25 m/s² in 7 steps. Particle image velocimetry (PIV) was adopted to evaluate the collapse behavior of slopes. Based on the PIV results, the distributions of ground displacement and shear strain were investigated. The strength parameters were determined by a direct box shear test and a vane shear test prior to the model tests. Subsequently, the modified Fellenius method was employed to study slope stability during earthquakes.

Keywords: Submarine landslide, Earthquake, Centrifuge model test, Clay, Slope stability analysis



1. Introduction

Tsunamis are not only generated by large earthquakes, but also by submarine landslides. In particular, submarine landslides generate destructive tsunamis and damage of coastal infrastructure [1, 2, 3]. The largest contributors to the height of a tsunami are the volume and velocity of the sliding mass [4, 5]. Therefore, to enable accurate predictions of tsunami elevation, it is important to elucidate the failure behavior of submarine slopes during earthquakes. Previous studies have suggested a Monte Carlo Simulation approach to assess the tsunami hazard generated by submarine landslides [6, 7, 8]. Such studies determined the potential slope failure by a slope stability analysis. However, little attention has been paid to the validity of applying a slope stability analysis to submarine slopes. Sento et al., [9] conducted a centrifugal model test to evaluate the applicability of the modified Fellenius methods to submarine slopes during earthquakes. The horizontal ground clay was prepared by consolidation, and the slope was shaped by cutting. Pseudo static forces were applied to the slopes. As a result, it was found that the modified Fellenius method is capable of accurately simulating the test results. However, the collapse behavior of a submarine slope during an earthquake remains unknown. The purpose of this study is to evaluate the collapse behavior of a submarine slope during an earthquake by performing a series of centrifugal model tests. Additionally, the validity of applying the modified Fellenius method to submarine slopes was investigated.

2. Centrifugal model tests

2.1 Outline centrifugal model tests

A rigid container (600 mm wide, 500 mm high, and 200 mm deep) was used for the tests. The centrifuge had a radius of 3.05 m, and an acrylic window enabled the observation of the seismic response by a camera (30 fps). Particle image velocimetry (PIV) was performed to evaluate the collapse behavior of slopes. Water pressure was applied to the model slopes by an upper water tank connected to the container. The test was performed at a centrifugal acceleration of 30 g.

2.2 Preparation of model slopes and test conditions

A schematic of the centrifuge model is shown in Fig. 1 (a), (b), and (c). The model slopes were constructed from clay by mixing AX kaolinite and MC clay in a ratio of 1:1 (by dry weight). The slope angles were 15°, 30°, and 35°. The physical properties of the clay are presented in Table 1. The model slopes were constructed according to the following procedure. First, clay with 100 % water content was poured into the container and consolidated by seepage pressure (0.23 MPa) at 1 g. Second, the clay was consolidated at the centrifuge acceleration of 30 g. Third, the model was spun down to 1 g, and shaped into a slope. Finally, colored sand was placed in a grid pattern on the side for measurements of displacement by PIV. Therefore, the model slopes were in an overconsolidated condition. Fig. 1 (d) shows the model slope of case 1. A series of tests were conducted at a centrifugal acceleration of 30 g with water depths of 15 and 23 m. The shaking events consisted of sinusoidal waves with 10 cycles at 80 Hz, with amplitudes from increasing 0.5 to 3.25 m/s² in 7 steps. Cases 1 and 3 were applied 7 times at amplitudes of 3.0 m/s². Case 2 was applied twice at amplitudes of 3.0 m/s², and 5 additional times at amplitudes of 3.0 m/s² for 50 cycles. The pore pressure was measured at the top of the model slopes, and the acceleration was measured on a shaking table.

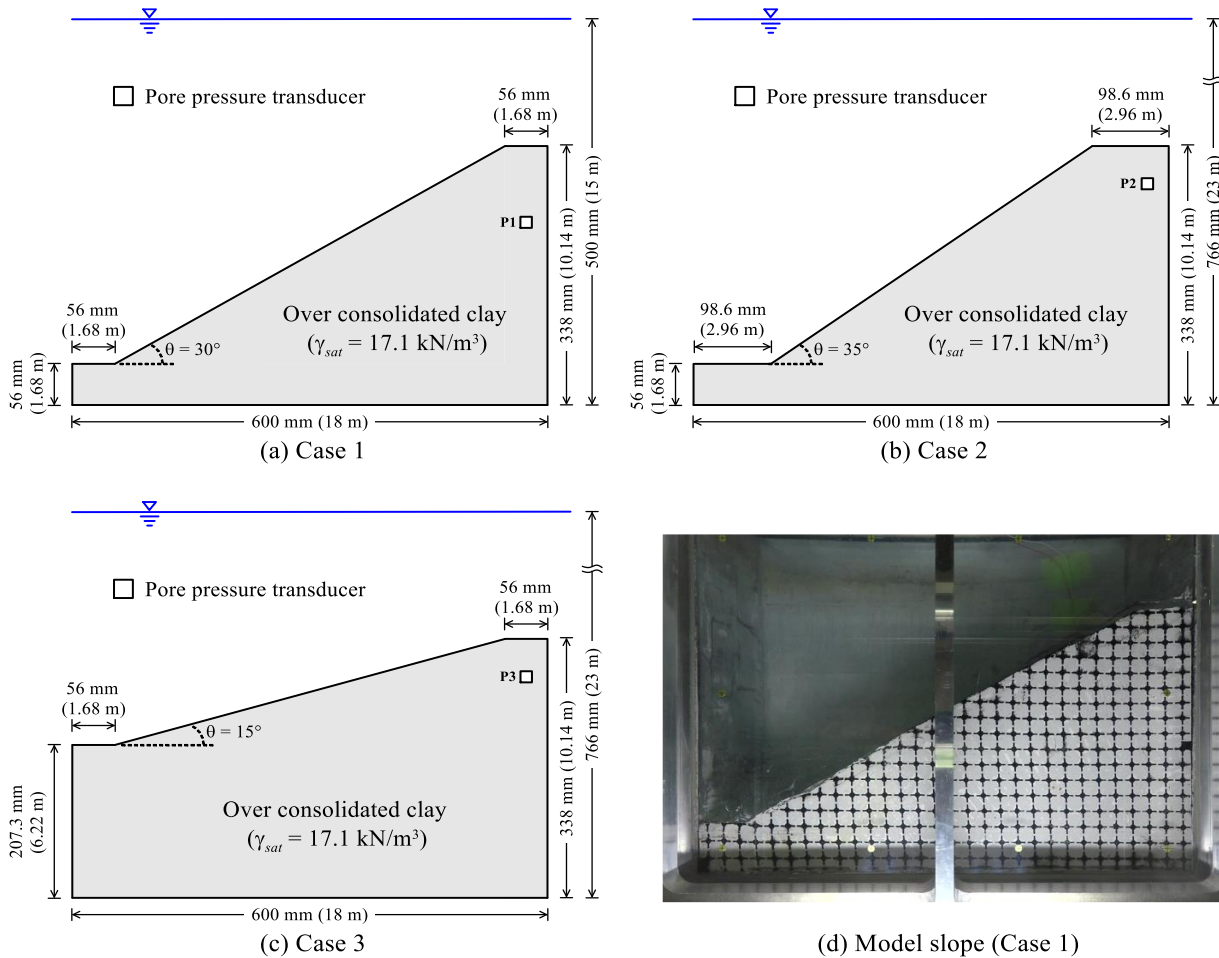


Fig. 1 – Schematic centrifugal model test (prototype) and model slope (Case 1)

Table 1 – Properties of clay

Properties	Value
Soil particle density ρ_s (g/cm ³)	2.739
Liquid limit w_L (%)	54.4
Plastic limit w_P (%)	37.0
Plastic index I_P	17.4

3. Centrifugal model tests results

3.1 Results of response of slope

The acceleration and pore water pressure time histories for cases 1–3 are illustrated in Fig. 2. In order to allow the pore water pressure to dissipate, intervals of five minutes were adopted during the dissipation



process. However, the time history of the interval is omitted from the figure. It can be observed that the pore water pressure fluctuates simultaneously with the shaking.

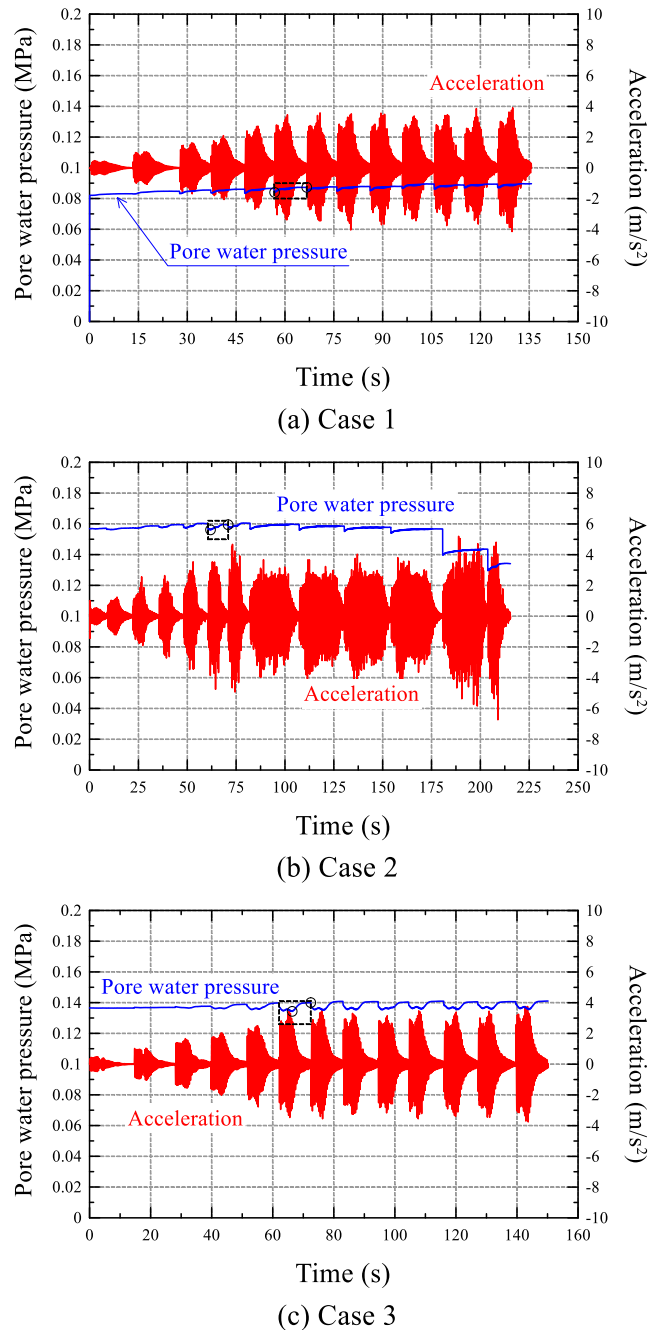


Fig. 2 –Acceleration and pore water pressure time history (Cases 1–3)

Fig. 3 shows enlarged views of the data from cases 1–3 at a shaking acceleration of 3.0 m/s^2 . Fig. 3 (a) shows that pore water pressure increases with fluctuation, and the excess pore water pressure, u_e , was 3.3 kPa (excess pore water pressure ratio, $r_{u_s} = 0.10$) during the shaking. Fig. 3 (b) and (c) show that the pore water pressure tendencies are similar in cases 2 and 3. The pore water pressure fluctuations were caused by dilative tendencies, because the model slopes were overconsolidated.

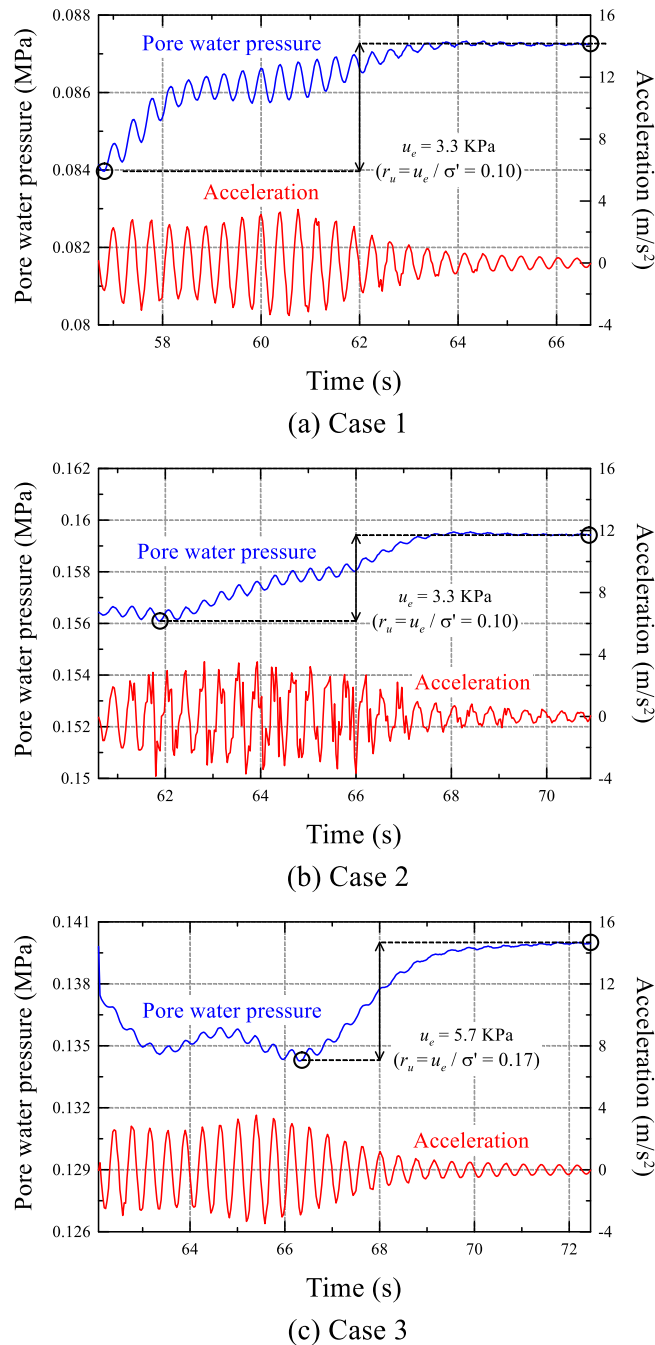


Fig. 3 –Pore water pressure on enlarged the area enclosed by the dotted line in Cases 1–3

3.2 Displacement and shear strain

Fig. 4 shows the displacement and shear strain of case 1. The red line in represents the slip surface determined by connecting the dots at which the shear strain reached approximately 10 %. Fig. 4 (a) indicates that shear strain has increased in the middle of the slope under the shaking acceleration of 2.5 m/s^2 . Shear deformation was observed at a relatively shallow depth. Moreover, the slip surface (Fig. 4 (b) to (d)) is deeper than those of the previous shaking events. Fig. 5 and 6 (Cases 2 and 3) show that displacement and shear strain indicate similar tendencies. Based on the above analysis, the slip surface was formed at a relatively shallow depth, and it became deeper as the shaking acceleration increased.

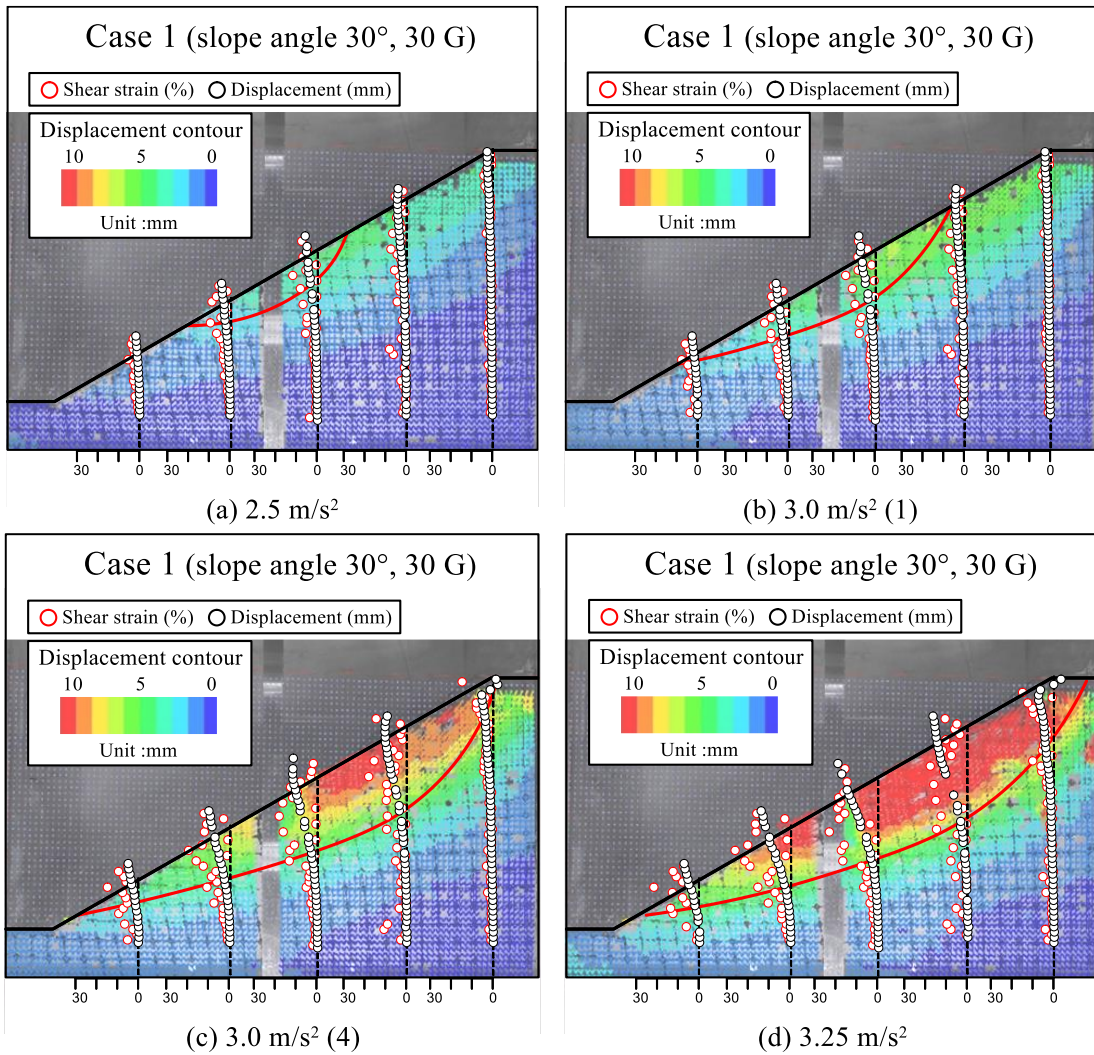


Fig. 4 –Displacement and shear strain (Case 1)

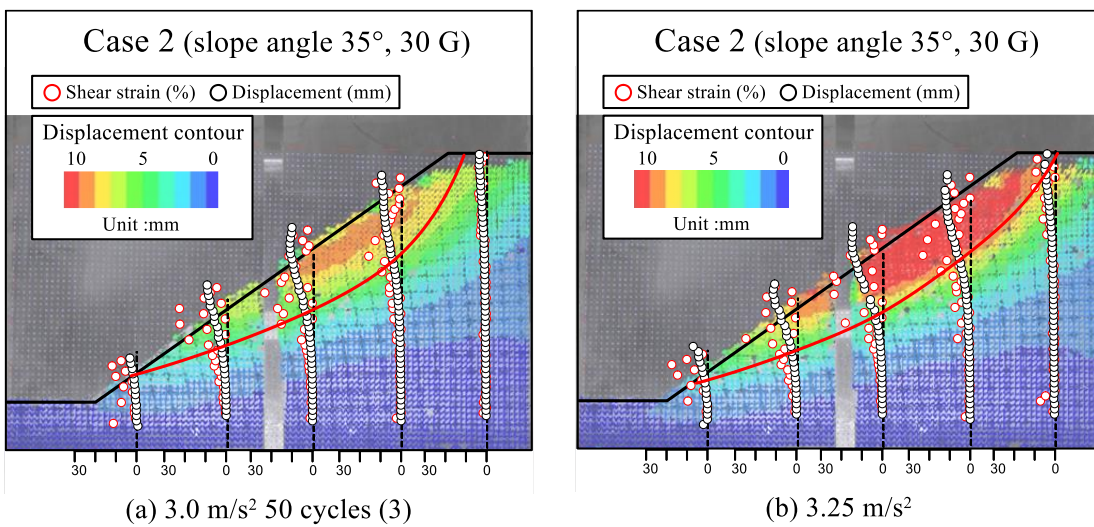


Fig. 5 –Displacement and shear strain (Case 2)

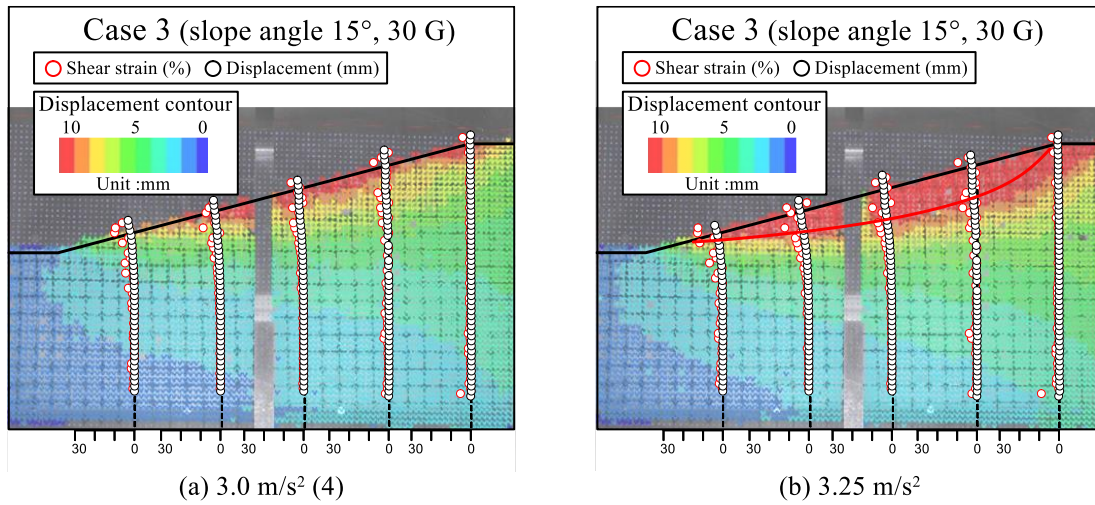


Fig. 6 –Displacement and shear strain (Case3)

4. Slope stability analysis during earthquake by modified Fellenius method

Slope stability analysis was performed using the modified Fellenius method in Eq. (1). Fig. 4 shows the outline of the modified Fellenius method.

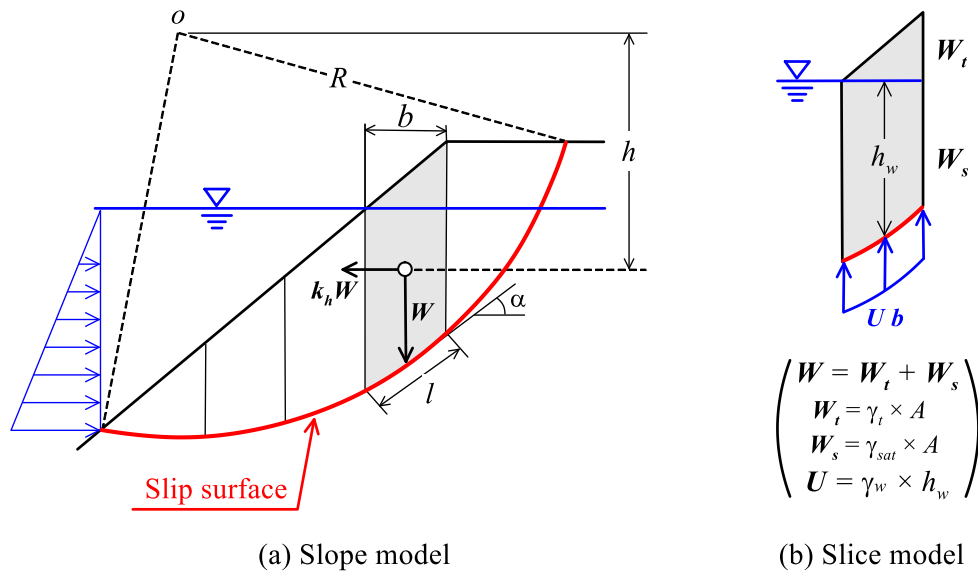


Fig. 7 –Outline of modified Fellenius method

$$F_s = R \Sigma \{cl + [(W - Ub)\cos\alpha - k_h W \sin\alpha] \tan\phi\} / \Sigma (RW \sin\alpha + k_h Wh) \quad (1)$$

where F_s is the safety factor, c is the cohesion, ϕ is the internal friction angle, R is the radius, A is the area of the slice, W is the weight of the slice, U is the pore water pressure at the bottom of the slice, γ_w is the unit weight of water, γ_t is the total unit weight of soil, γ_{sat} is the saturated unit weight of soil, and k_h is the horizontal seismic coefficient.



4.1 Determination of strength parameters

Fig. 8 shows the vane shear test before and after the model test and the unconfined compression test after the model test, which were performed at 1 g. The shear strength increases as with increasing. The shear strength in the model at 30 g increases with increasing effective confining pressure. Therefore, it is necessary to correct the shear strength and ϕ_{cu} . Fig. 9 shows test results of 1 g and the corrected value of 30 g. The corrected value is evaluated by Eq. (2):

$$s_u = s_{u0} + \sigma'_v \tan \phi_{cu} \quad (2)$$

where s_u is the undrained shear strength, s_{u0} is the measured undrained shear strength at 1 G in the slope, σ'_v is effective confining pressure at 30 G in the slope, and ϕ_{cu} is the internal friction angle of the overconsolidated clay determined by a direct box shear test. The strength parameters were determined by a linear approximation between the effective confining pressure and the shear stress.

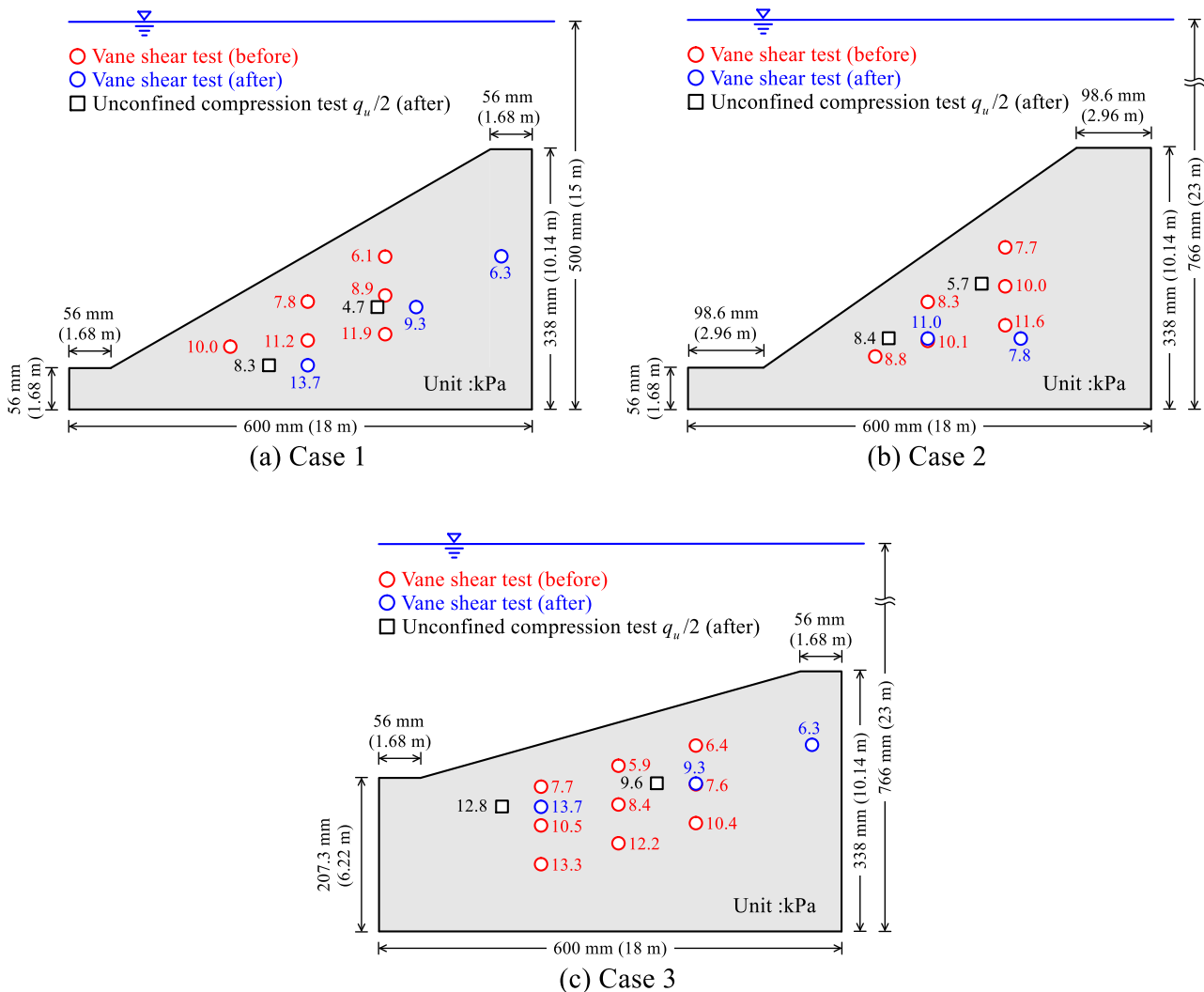
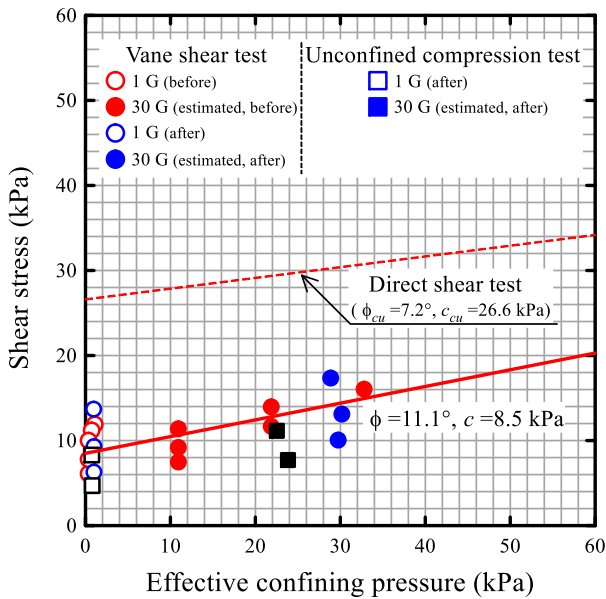
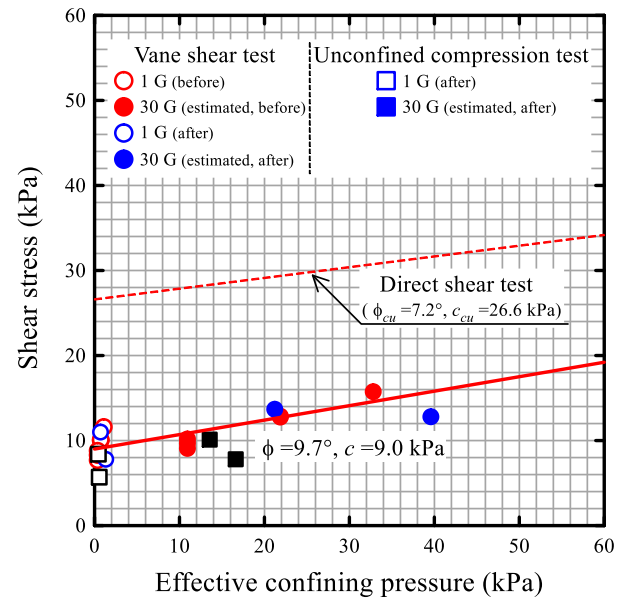


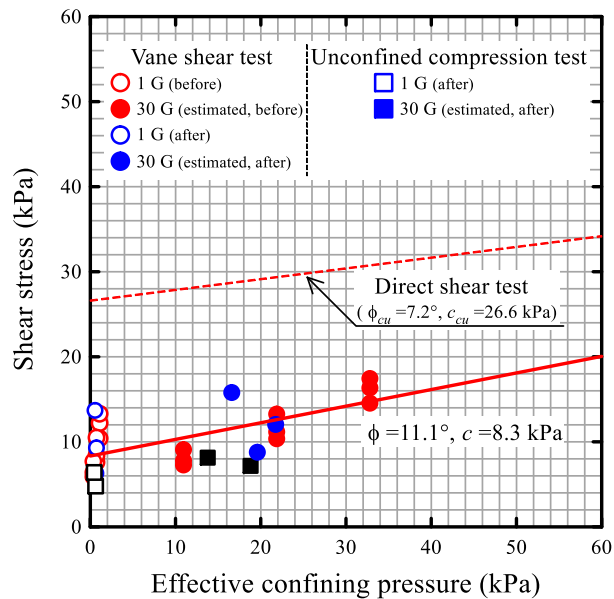
Fig. 8 – Shear strength before and after shaking test



(a) Case 1



(b) Case 2



(c) Case 3

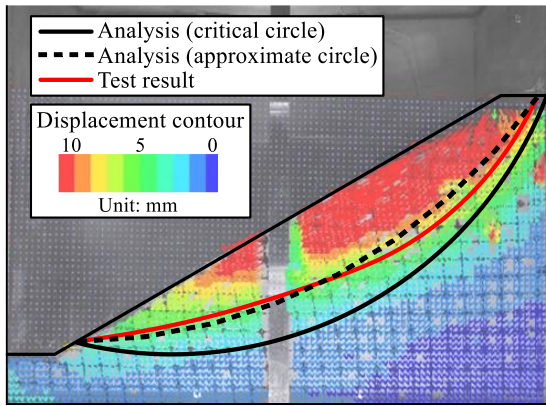
Fig. 9 –Strength parameters determined by a direct shear test and vane shear test before the model tests

4.2 Analysis results and discussion

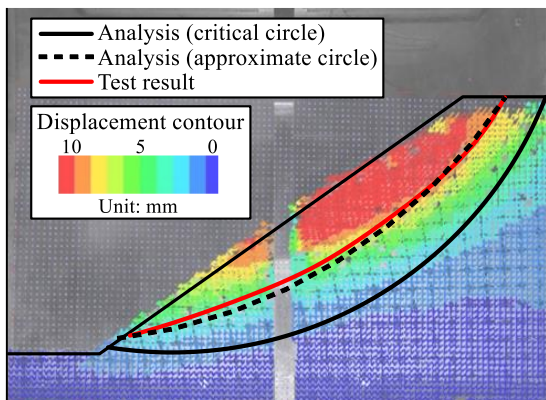
The slip surface observed in the test and used for the analysis are illustrated in Fig. 10. The critical circle with the minimum safety factor (F_s) appears deeper than the test results. Fig. 11 shows the relationship between the seismic coefficient and F_s value of the approximated and critical circles. The F_s value is smaller than 1 at the beginning of slope collapse in cases 1 and 2. The F_s value is almost equal to 1 at the collapse in case 3. Therefore, the modified Fellenius method is reasonably applied to the problem of a submarine slope during an earthquake. The sliding mass volume of the critical circle is larger than that observed in the model



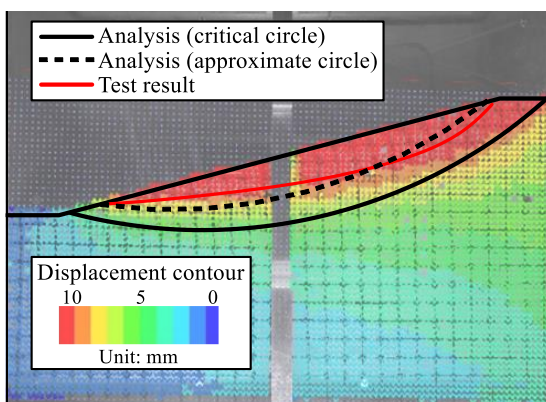
tests. From a practical point of view, the critical circle is plausible for conservatively estimating the tsunami height.



(a) Case 1 (slope angle 30°, 3.25 m/s²)

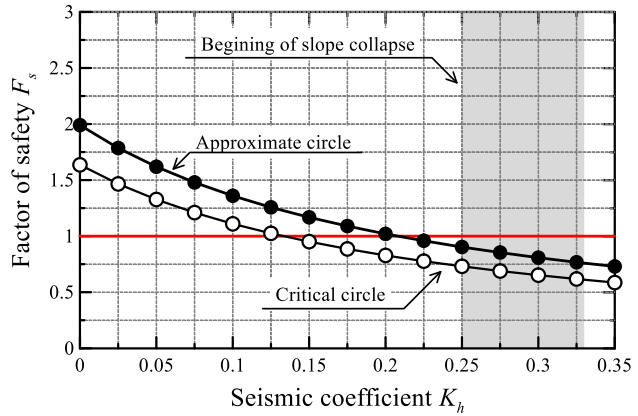


(b) Case 2 (slope angle 35°, 3.25 m/s²)

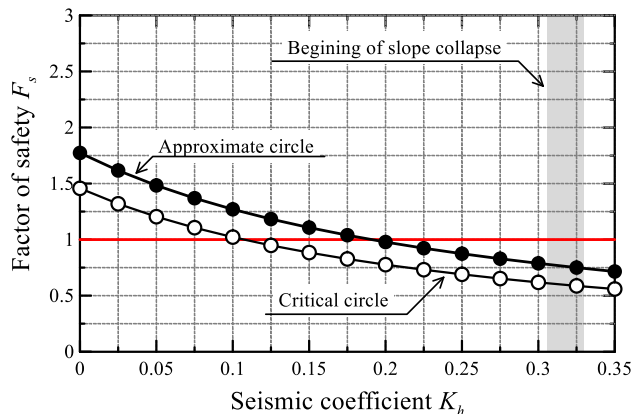


(c) Case 3 (slope angle 15°, 3.25 m/s²)

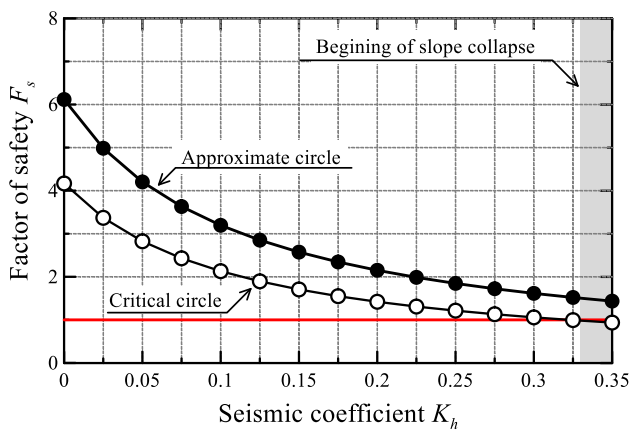
Fig. 10 – Relationship between factor using modified Fellenius method



(a) case 1 (slope angle 30°)



(b) case 2 (slope angle 35°)



(c) case 3 (slope angle 15°)

Fig. 11 – Test result and slip surface of safety and seismic coefficient



5. Conclusion

We evaluated the collapse behavior of a submarine slope during an earthquake by performing a series of centrifugal model tests. Additionally, the validity of applying a modified Fellenius method to submarine slopes was investigated. The results of this study can be summarized as follows:

- 1) The pore water pressure increases with fluctuation during shaking.
- 2) The slip surface is formed by a deformation occurring at a relatively shallow depth, and it becomes deeper with increasing shaking acceleration.
- 3) The location of the critical circle with minimum factor of safety (F_s) is deeper than that in the test results.
- 4) From a practical point of view, the critical circle by the modified Fellenius method is plausible for conservatively estimating tsunami height.

6. Acknowledgements

This research was carried out in the commissioned project of the Japan Nuclear Regulation Authority on 2018.

7. References

- [1] Tappin DR, Watts P, Grilli ST (2008): The Papua New Guinea tsunami of 17 July 1998: anatomy of a catastrophic event. *Nat. Hazards Earth Syst. Sci.*, **8**, 243-266.
- [2] Matsumoto H, Baba T, Kashiwase K, Misu T, Kaneda Y (2009): Discovery of submarine landslide evidence due to the 2009 Suruga Bay earthquake. In: Yamada Y. et al. eds., *Advances in Natural and Technological Hazards Research*, 31, Springer, 549-559.
- [3] Sassa S, Takagawa T (2019): Liquefied gravity flow-induced tsunami: first evidence and comparison from the 2018 Indonesia Sulawesi earthquake and tsunami disasters. *Landslides*, 16(1), 195-200.
- [4] Watts P, Grilli ST, Tappin DR, Fryer GJ (2005): Tsunami generation by submarine mass failure. II: predictive equations and case studies., *J. Waterw. Port Coast. Ocean Eng.*, **131**(6), 298-310.
- [5] Masson DG, Harbitz CB, Wynn RB, Pedersen G, Lovholt F (2006): Submarine landslides: processes, triggers and hazard prediction. *Phil. Trans. R. Soc. A*, **364**, 2009-2039.
- [6] Grilli ST, Taylor ODS, Baxter CDP, Marezki S (2009): A probabilistic approach for determining submarine landslide tsunami hazard along the upper east coast of the United States, *Marine Geology*, **264**, 74-97.
- [7] Shigihara Y, Horrillo J (2014): A Probabilistic Methodology for Determining Tsunami Sources Generated by Submarine Landslide -Application to the Gulf of Mexico-, *Journal of Japan Society of Civil Engineers, Ser. B2 (Coastal Engineering)*, 70(2), I_281-I_285 (in Japanese).
- [8] Pampell-Manis A, Horrillo J, shigihara, Parambath L (2016): Probabilistic assessment of landslide tsunami hazard for the northern Gulf of Mexico, *Journal of Geophysical Research: Oceans*, 121(1), 1009-1027.
- [9] Sento N, Unno T, Nakamura S (2017): Preparation for slope model simulates submarine ground and its stability evaluation, *Journal of Japan Society of Civil Engineers, Ser. B3 (Ocean Engineering)*, 73(2), I_306-I_311 (in Japanese).